Combustion and Flame 258 (2023) 113015

Contents lists available at ScienceDirect

Combustion and Flame

journal homepage: www.elsevier.com/locate/combustflame

Multi-target active subspaces generated using a neural network for computationally efficient turbulent combustion kinetic uncertainty quantification in the flamelet regime

Benjamin C. Koenig, Sili Deng*

Department of Mechanical Engineering, Massachusetts Institute of Technology, 77 Massachusetts Avenue, Cambridge, MA 02139, USA

ARTICLE INFO

Article history:
Received 8 May 2023
Revised 11 August 2023
Accepted 11 August 2023
Available online 14 September 2023

Keywords:
Uncertainty quantification
Active subspace
Turbulent combustion
Flamelet
Deep neural network

ABSTRACT

Propagating uncertainties in kinetic models through combustion simulations can provide important metrics on the reliability and accuracy of a model, but remains a challenging and numerically expensive problem especially for large kinetic models and expensive turbulent combustion simulations. Various surrogate model and dimension reduction techniques have previously been applied in order to reduce the cost of forward uncertainty propagation in combustion simulations, but these are often limited to low-dimensional, simple combustion cases with scalar solution targets. In the current work, we developed a neural network-accelerated framework for identifying a low-dimensional active kinetic subspace that applies to the entire temperature solution space of a flamelet table and can capture the mixture fraction and strain rate dependent effects of the kinetic uncertainty. We then demonstrated the computational savings enabled by this framework through a proof-of-concept, flamelet-based application in a Reynolds-averaged Sandia Flame D simulation using a chemical model for methane combustion with 217 reactions. By leveraging the large dimensional compression and low-cost scaling of the active subspace method, offloading the initial dimension reduction gradient sampling onto the laminar flamelet simulations, and accelerating the gradient sampling process with a specifically designed neural network, we were able to estimate the temperature uncertainty profiles across the solution space of the turbulent flame with strong accuracy of 70 – 85% using just seven perturbed solutions. Additionally, as it occurs entirely within the flamelet table, the cost of identifying the reduced subspace does not scale with the cost of the turbulent combustion model, which is a promising feature of this framework for future application to larger-scale and more complex turbulent combustion applications.

1. Introduction

The chemical model is an integral part of turbulent combustion simulations. Whether utilizing detailed or reduced chemistry, any uncertainties present will propagate forward through the combustion models and can result in substantial uncertainties in the simulation results [1–3]. These output uncertainties and their sensitivities to model parameters are a key component in evaluating model results [4–6] and are often found to be large enough to account for nearly the entire discrepancy between the simulations and the experimental data [1,7]. While quantifying the effects of kinetic uncertainties on the accuracy and precision of combustion simulations are important, such effort is often expensive to carry out on a meaningful scale.

The key challenge for uncertainty quantification in practical turbulent combustion simulations is the high computational cost associated with the simulations, which makes the forward problem expensive. Two main categories of methodology have been commonly applied in combustion research to alleviate the high computational expense. The first involves building low-cost surrogate models to replace the physical simulation. Polynomial chaos expansions (PCE) and high-dimensional model representations (HDMR), for example, are often used to leverage a relatively small number of expensive simulations in the construction of surrogate models, which can be efficiently sampled in the forward uncertainty problem [7,8]. However, these methodologies suffer from the “curse of dimensionality”, making their construction inefficient in problems with a large kinetic model [9–11]. Local sensitivity analyses and screening methods [12–15] as well as newer artificial neural network-based surrogate methods [11,16] are often used either to reduce the input space for the response surface algorithms or accelerate their computation. Due to the substantial amount

* Corresponding author.
E-mail address: silideng@mit.edu (S. Deng).

https://doi.org/10.1016/j.combustflame.2023.113015
0010-2180/

of training data required from the physical solver, however, such response surface-based methodologies are typically used only in cheaper, low-dimensional combustion cases such as ignition delay [7,8], laminar flame speed [17,18], or flow reactor [17] simulations, rather than complex flow fields.

The second category involves methods that solve the forward problem directly in the physical solver, but leverage various techniques to reduce the total number of simulations needed. These are especially useful in expensive turbulent simulations where response surfaces cannot be feasibly constructed. The simplest approach might leverage the previously discussed local sensitivity analysis to deduce a reduced set of highly sensitive uncertain parameters for forward propagation with fewer samples than the full set. The cost associated with this can still become large, however, since the identification of the reduced set can again suffer from the high-dimensional kinetic parameter space and the reduced set itself may still contain on the order of ten or more sensitive reactions that must be sampled. Mueller et al. [1] proposed a physics-informed dimension reduction based on the flamelet approach for turbulent combustion modelling that can further reduce the cost of the forward kinetic uncertainty quantification. The uncertainty was first propagated from the kinetic model to the low-dimensional flamelet table, and then further simplified down to a single uncertain flamelet solution variable. In doing so, the computational expense of discovering a reduced kinetic space was offloaded to the cheap one-dimensional laminar flamelets. The turbulent combustion large eddy simulation uncertainty was then characterized remarkably efficiently by sampling this one-dimensional uncertain input instead of directly sampling a series of ten or more sensitive kinetic parameters, delivering further savings in the forward propagation step. The assumptions made to facilitate such a reduction were grounded in theory yet not rigorously examined, likely due to the large computational cost of each turbulent simulation. The active subspace method [2,9,19] is another approach for identifying reduced kinetic spaces for efficient sampling. Unlike traditional methods that identify an active subset of important reactions, this algorithm identifies active linear combinations of important reactions (active subspaces) that most impact the quantity of interest. This is similar to principal component analysis, though it identifies directions in the gradient space and thus in the input kinetic parameters, rather than the output state vectors [20], and performs such a reduction globally across the entire uncertainty space, rather than locally at the nominal values [21]. The coupled information contained in each of these subspace directions allows for greater reduction than typical sensitivity analyses or response surface-based methods, often down to even a single subspace direction [2,9,22,23], and thus greater computational savings in the forward propagation step. The active subspace method is particularly useful in problems with high input dimension, as is often the case with chemical kinetic uncertainty, since it partially avoids the curse of dimensionality thanks to its relatively low dependence on input dimension size [24,25]. This is especially true for problems with low-dimensional active subspaces, which are investigated in this work.

Previous combustion applications of the active subspace algorithm have typically investigated only a single quantity of interest at a time such as liftoff height [2,22], ignition delay time [2,22,26], combustor exit pressure [27], or scalar soot metrics [23]. Ji et al. [9] expanded on this by investigating shared low-dimensional kinetic subspaces that were capable of representing the kinetic uncertainty across multiple target quantities. Various active subspace works have also leveraged and validated physics-informed simplifications of kinetic uncertainty (similar to [1]) in various configurations, such as ignition delay time as a predictor of liftoff height [2,22]. Such applications benefit both from the greater dimensional compression of the active subspace method, as well as the ability to sample gradients for the identification of such subspaces in cheaper, lower-dimensional problems. The combination of multi-target active subspaces and a physics-informed kinetic uncertainty simplification was proposed in Koenig et al. [28], where a low-dimensional subspace was found to accurately represent the kinetic uncertainty across the entire temperature profile of a laminar flamelet. While meaningful, this result was limited to a single flamelet and did not investigate the full flamelet table required to apply the subspace to a turbulent simulation, inspiring further work in this area of multi-target, physics-informed kinetic subspace identification.

In this work, we proposed and demonstrated a complete forward kinetic uncertainty propagation framework for turbulent combustion in the flamelet regime, starting from an uncertain model and ending with turbulent simulation uncertainty profiles. We leveraged an artificial neural network surrogate model to accelerate the active subspace reduction process, which was performed here on the full two-dimensional coordinate space of a flamelet table. The inexpensive gradients sampled from this neural network were used to reduce the high-dimensional kinetic uncertainty of the entire flamelet table into a low-dimensional active subspace. We then quantified the effects of kinetic uncertainty on the simulation of Sandia Flame D and compared output uncertainty profiles obtained via efficient sampling in the active subspace and via brute force Monte Carlo sampling in the full kinetic space. This framework operates efficiently on both ends of the problem at hand - it identifies a remarkably low dimension kinetic uncertainty space that applies across a much broader input space than what is typically investigated in combustion uncertainty research. This scale of reduction, demonstrated through the two-dimensional, Reynolds-averaged turbulent combustion simulation shown here, has the potential to be scaled up to facilitate forward uncertainty propagation in more expensive cases, such as large eddy simulations.

2. Methods

In this work, we innovate on the kinetic subspace investigation method originally applied to the uncertainty quantification of a single nonpremixed methane flamelet in [28] by applying it across a complete flamelet table, taking into account strain rate in addition to kinetic parameter uncertainty and mixture fraction. This novel expansion enables the direct application of the reduced kinetic subspace in the forward uncertainty propagation of the complete temperature profile of a nonpremixed turbulent flame simulation. The methodologies used for these two steps are detailed in Sections 2.1 and 2.2, respectively. An overview of this framework, which leverages the kinetic similarity among the flamelets representing the thermochemical states of the turbulent flame, is presented in Fig. 1 along with a summary of its key advantages compared to standard sensitivity-based forward propagation. The following subsections describe each step in detail.

2.1. Kinetic subspace discovery

We begin with a discussion of the active subspace algorithm, specific details of which motivate construction of a neural network surrogate model (described later in this section). The generic algorithm, methodology, proofs, and kinetic discussion for the active subspace method are presented in [19] and [28]. Here, we summarize the application in this work.

All flamelet data used for subspace discovery was generated in Cantera [29] using a tailored form of the GRI-Mech 3.0 model [30] with 217 reactions neglecting NO chemistry. All uncertain kinetic parameters are perturbed within the ranges given in the lit-

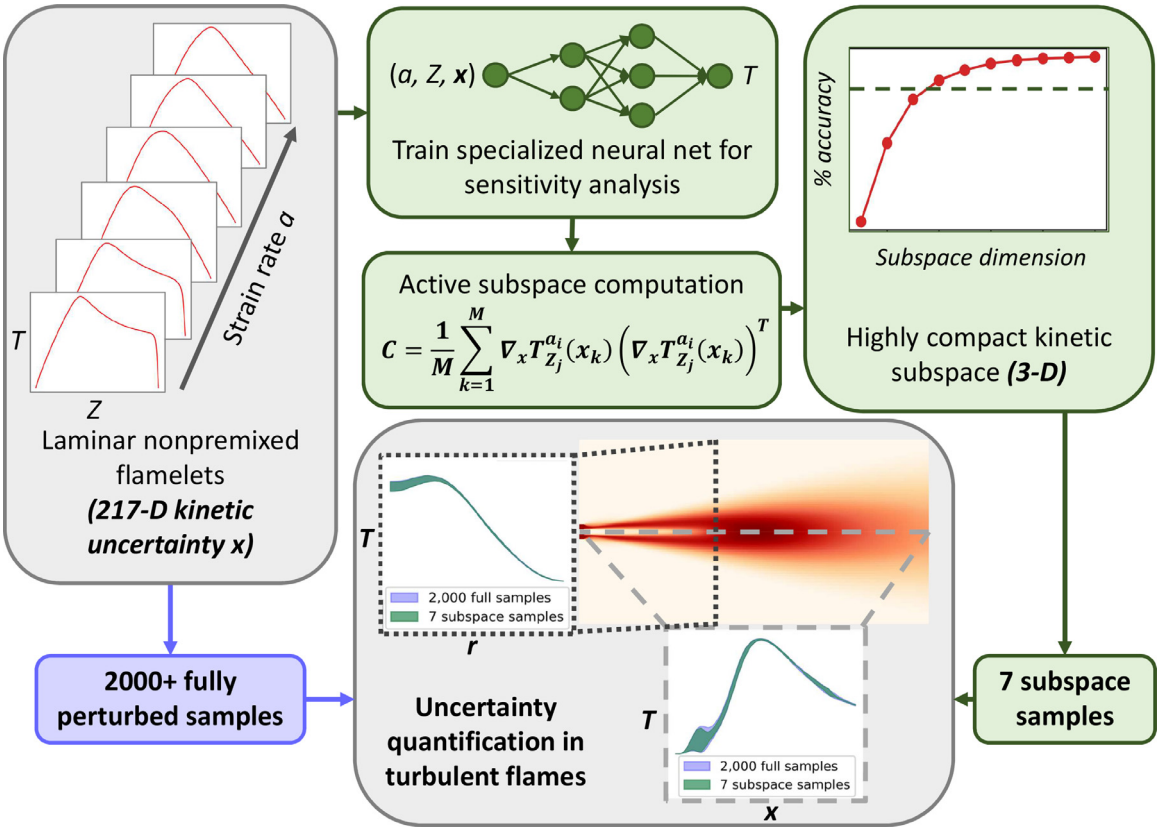

Fig. 1. Overview of the methodology used to efficiently propagate kinetic uncertainty in this work. The 217-dimensional kinetic uncertainty is reduced across the entire flamelet table to a three-dimensional active subspace within which efficient sampling for forward propagation is performed. Accuracy benchmarking is then done against a much larger sample (2,000 samples) of fully perturbed models. Highlighted here are key advantages of the proposed framework including large dimensional compression and kinetic reductions that are applicable to the entire turbulent flame profile.

erature [31],

$$x_\ell = \frac{\ln k_\ell / k_{\ell,0}}{\frac{1}{3}\ln u_\ell} \sim N(0,1), \tag{1}$$

where x_ℓ is the ℓth index of the normalized rate constant perturbation vector $\mathbf{x}$, k_ℓ is the perturbed value of the ℓth rate constant, $k_{\ell,0}$ is the nominal value of the ℓth rate constant, u_ℓ is the uncertainty factor corresponding to $k_{\ell,0}$ as reported in [31], and $N(0,1)$ denotes the standard normal distribution with zero mean and unit variance. We additionally use the following mean strain rate formulation throughout our discussion of the flamelets for consistency,

$$a = (Q_{fuel} + Q_{oxidizer})/2d, \tag{2}$$

where Q is the volumetric flow rate on either the fuel or oxidizer side, and d is the width of the counterflow domain. Finally, we define the hydrogen mixture fraction Z identically to [28] as

$$Z = \frac{Y_{\text{mix}} - Y_{\text{ox}}}{Y_{\text{fuel}} - Y_{\text{ox}}}, \tag{3}$$

where Z is the mixture fraction at a given location, and Y_{mix}, Y_{ox}, and Y_{fuel} represent the hydrogen mass fractions of the mixture, oxidizer stream, and fuel stream, respectively.

The aim of the kinetic subspace discovery process is to identify an r_u-dimensional subspace in the d-dimensional kinetic rate constant space (with $r_u << d$) that describes the bulk of the temperature variation across an arbitrarily strained flamelet, at any given mixture fraction. That is, at any strain rate a and mixture fraction Z, the goal of the subspace is to accurately approximate the temperature response T_Z^a to any kinetic perturbation,

$$T_Z^a(\mathbf{x}_d) \approx T_Z^a(\mathbf{x}_{r_u}), \tag{4}$$

where $\mathbf{x}_d$ is a full-rank vector of rate constant perturbations for the d reactions in the kinetic model, while $\mathbf{x}_{r_u}$ is the same vector expressed with only the r_u basis directions present in the subspace. Such a reduction allows for forward sampling in just r_u dimensions, which given $r_u << d$ indicates large savings for forward uncertainty propagation. In order to identify the subspace that applies globally in Eq. (4), we begin with a traditional single-target subspace, where for a fixed strain rate a_i and a fixed mixture fraction Z_j, the quantity of interest is the scalar flamelet temperature $T_{Z_j}^{a_i}$. Applying the standard active subspace algorithm we can compute the matrix $\mathbf{C}$ and its eigendecomposition following

$$\mathbf{C} = \frac{1}{M}\sum_{k=1}^{M} \nabla_x T_{Z_j}^{a_i}(\mathbf{x}_k)(\nabla_x T_{Z_j}^{a_i}(\mathbf{x}_k))^T = \mathbf{W}\Lambda\mathbf{W}^T. \tag{5}$$

Here, M is the total number of rate constant samples k that we generate from the full uncertainty space in $\mathbf{x}$, with the gradient $\nabla_x T_{Z_j}^{a_i}(\mathbf{x}_k)$ evaluated once per iteration k. We compute a separate local subspace at each strain rate and mixture fraction location (i, j) in the flamelet table, and as in [28] extract the leading eigenvector $\mathbf{w}_{1,(i,j)}^{local}$ as the one-dimensional subspace. We use the local superscript here to denote a subspace that applies locally to a single location in the flamelet phase space. However, by virtue of the M samples in Eq. (5) across the entire kinetic uncertainty space, this single-target subspace is itself a global sensitivity measure.

We then define $\mathbf{A}$ as the $(n_i * n_j) \times d$ matrix of all 1-D local subspaces $\mathbf{w}_{1,(i,j)}^{local}$, where n_i and n_j are the total number of strain rate and mixture fraction locations, respectively, and each row of $\mathbf{A}$ is the corresponding $1 \times d$ local subspace vector computed in Eq. (5). $\mathbf{A}$ therefore has a very large aspect ratio, where each column rep-

resents a specific chemical reaction and each row is that reaction's contribution to a single local subspace. Depending on the results of Eq. (5) it is also possible to use multi-dimensional local subspaces in the construction of **A**. We choose to use one-dimensional local subspaces here based on the results of [28] as well as later discussion in Section 3.1. As in [28], though this time with n_i times more rows, we take the singular value decomposition (SVD) of **A**,

$$\mathbf{A} = \mathbf{USV}^T, \tag{6}$$

where **S** is an $(n_i * n_j) \times d$ diagonal matrix with d singular values σ that correspond to the relative importance of the principal directions **V**. The squared singular values σ^2 relate to the eigenvalues of the matrix $\mathbf{AA}^T$, and are used to decide r_u, the dimension of the final subspace, based on their relative magnitudes. After selecting r_u, we extract from **V** a reduced space $\mathbf{w}_m$ with m ranging from 1 to r_u. More detailed discussion into the selection process and physical interpretation involved with Eqs. (5) and (6) are provided in [28]. Here, we emphasize the key generalization of this work in the $(n_i * n_j)$ sized **A** matrix that includes both the mixture fraction and strain rate input spaces of the flamelets. Thus, the final r_u-dimensional subspace discovered here describes the kinetic uncertainty of the entire two-dimensional input space of a flamelet table, in contrast with the one-dimensional mixture fraction space investigated in [28] (or the zero-dimensional quantities of interest typically examined with the generic active subspace method).

The active subspace method partially avoids the curse of dimensionality thanks to its low dependence on input dimension size [9]. The use of one-dimensional local subspaces further decreases the subspace generation cost in Eq. (5) [24,25]. However, due to the two-dimensional flamelet input space investigated, $\sim 10^4$ local subspaces are required to construct **A** in Eq. (6). The absolute lowest possible number of gradient evaluations per local subspace is 22 as per the generic dimensional scaling proposed in [25]. A more reasonable number based on the same scaling laws with mid-range parameters is 100, while the scaling rules typically used in combustion applications [2,23] would call for over 1000 based on the large dimensionality of the kinetic problem investigated here. We therefore expect a grand total of gradient evaluations on the order of $10^6 \sim 10^7$. To reduce the computational cost associated with gradient computation we use a neural network surrogate model with a physics-based structure inspired by Nonlinear Independent Dual Systems [32] and Deep Operator Networks (DeepONet) [33]. Artificial neural networks have been found to be more efficient than PCE and HDMR response surfaces for a kinetic uncertainty problem of similarly large dimension as the methane model investigated here [34], and are also well-suited to efficient gradient evaluation by virtue of the backpropagation algorithm [35], as argued and demonstrated in [28]. Deep artificial neural networks have been proposed recently as an efficient method for flamelet tabulation [36], and DeepONet-type networks have also seen use in various recent combustion applications [28,37,38]. The network structure used here, shown in Fig. 2, is similar to that used in [28]. Key features include grid independence, where the inclusion of mixture fraction and strain rate as input nodes allows for training on data with arbitrarily refined grids and then downstream application on a single grid for consistency; and inductive bias, where the splitting of the two fundamentally different inputs (kinetics and boundary conditions vs. flame sampling location) encodes existing physical knowledge of the problem's structure into the network, potentially easing the burden of learning the remaining physics and thus of training the network. The key difference here is the strain rate parameter input node, which allows the network to learn (and compute gradients for) the entire flamelet table, rather than just a single flamelet.

The hyperparameters of this network were selected using the Ray Tune package [39], which performs an optimized grid search across user-specified ranges of hyperparameters to improve overall network performance. In this case, 100 networks were tested for up to 100 epochs each, with each composed of a random sample of 4 to 256 nodes per layer, 2 to 20 parameter layers, 2 to 20 coordinate layers, a learning rate of $1 * 10^{-4}$ to $1 * 10^{-3}$, and a batch size of 32 to 512. The final network, chosen based on performance in this grid search, comprised 13 parameter layers and 6 coordinate layers of 128 nodes each. The learning rate and batch size were $1.1 * 10^{-4}$ and 256, respectively. Residual skip connections [40] every two layers were used in both sub-networks. Flamelet solution training data was generated using the GRI-Mech 3.0 model [30] in Cantera [29] in the counterflow configuration using fuel composition and temperature boundary conditions that match the turbulent case (discussed in Section 2.2). Datasets were computed across a large range of strain rates from $3 * 10^{-2}$ 1/s to near-extinction at $3 * 10^2$ 1/s, defined here using the formulation in Eq. (2). Scaling rules for rapid convergence across the strain rate coordinate were taken from [41]. Sigmoid-weighted linear units [42] were used as activation functions, and the ADAM optimizer [43] with a weight decay of $1 * 10^{-4}$ was used to update the network parameters.

Finally, with gradients evaluated in a trained neural network surrogate model and the active subspace algorithm as described in Eqs. (5) and (6), we are able to compute the r_u-dimensional subspace that is applied to the forward problem in the turbulent nonpremixed combustion simulation described in Section 2.2. This subspace is expressed as a linear combination of kinetic parameters, making it directly applicable to forward uncertainty quantification in any turbulent simulation using the same boundary conditions and chemical model. In this case, however, we investigate only the most direct and theory-supported application to a flamelet-based turbulent combustion simulation to demonstrate the methodology's accuracy at a reasonable computational cost.

2.2. Benchmark turbulent flame simulation details

A two-dimensional axisymmetric model of the piloted Sandia Flame D [44] was used to evaluate the applicability of the flamelet-derived subspace to a multidimensional turbulent simulation. Such application of a kinetic subspace directly to the full temperature profile of a turbulent simulation has not been previously reported in the literature to our knowledge, and is made possible by the expanded methodology developed in this work. The flame configuration involves a $7.2 * 10^{-3}$ m diameter partially premixed fuel jet of 25% methane and 75% dry air (by volume) surrounded by a $18.4 * 10^{-3}$m pilot of hot combustion products (taken as Z=0.27 as per [45]), with an outer co-flow of cold air. The velocities of these three flows are 49.6 m/s, 11.4 m/s, and 0.9 m/s, respectively. The inlet temperatures are 294 K, 1880 K, and 291 K, respectively. The final mesh used to investigate the forward problem, as well as a general description of the computational domain, is shown in Fig. 3.

We construct a standard, straightforward, and relatively inexpensive model for application in forward uncertainty propagation leveraging various previously examined and verified methods for the Sandia Flame D [46–48]. A stretched grid of 24,180 cells (Fig. 3) is used to discretize the 1.2 m $\times$ 0.3 m computational domain. The flame is simulated using the realizable $k-\epsilon$ model. The realizable model differs from the standard $k-\epsilon$ model in its formulation of the dissipation rate and eddy viscosity equations, and was originally proposed and later applied to the Sandia Flame D [46,49] for its improved spreading rate performance in axisymmetric jet flame simulations. Standard values [49] of the constant C_2 as well as the turbulent kinetic energy and dissipation rate Prandtl numbers σ_k and σ_ϵ are taken as 1.9, 1.0, and 1.2, respectively. The choice of a RANS model was made to reduce the cost of the simulation

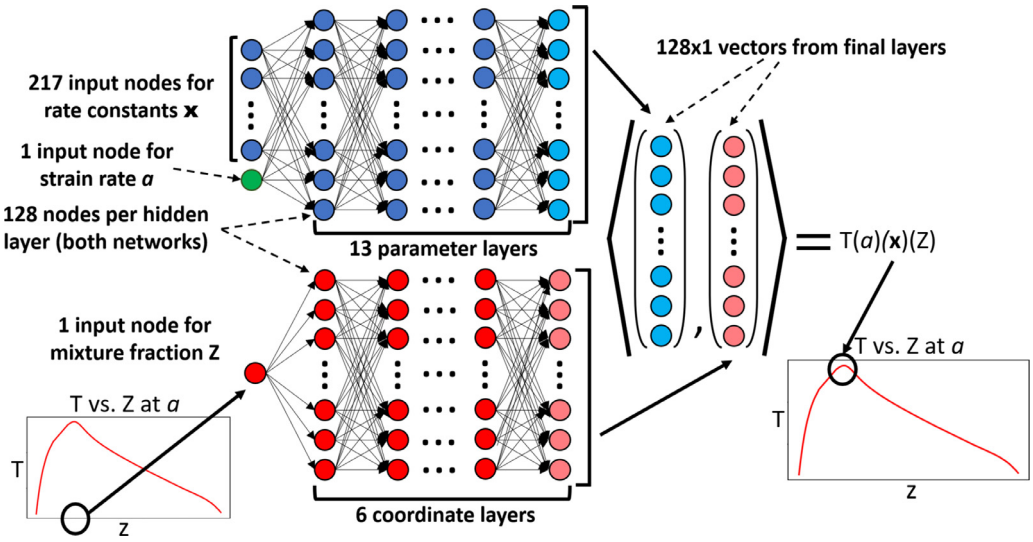

Fig. 2. Neural network surrogate model for flamelet simulations to accelerate sensitivity computations. The parameter and coordinate branches are independent until the last layer in which their results are combined via inner product to arrive at a final temperature prediction. Residual skip connections every two layers are not shown to maintain clarity. Training occurs independently of discretization, and the network can be evaluated on any inputs Z and a in an arbitrary grid.

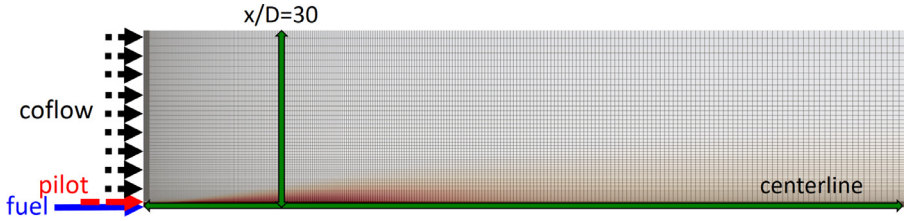

Fig. 3. Stretched axisymmetric computational mesh used for Sandia Flame D simluations, with nominal temperature profile overlaid in red for visualization. Green arrows in mesh show profile sampling locations used for forward propagation visualization and metrics in Figs. 11 and 12. (For interpretation of the references to colour in this figure legend, the reader is referred to the web version of this article.)

and enable accuracy comparisons between subspace samples and full kinetic space samples. The inexpensive RANS model enables mostly-converged exploration of the full kinetic uncertainty space directly in the turbulent flame, which establishes an estimate of the ground truth of the kinetic uncertainty effect on the temperature profile. An LES model would have resulted in more accurate model predictions, but based on a computational cost on the order of 10,000 CPU hours per simulation [1], would not have allowed for similar ground truth comparisons. That being said, the kinetic reduction methodology of Section 2.1 is not restricted to any specific turbulence model, so while a RANS model is used here for proof-of-concept demonstration and accuracy evaluation purposes users can alternatively propagate the reduced kinetic models forward through an LES simulation if better-resolved turbulence effects are desired.

Following the flamelet-based uncertainty method (and similarly to [47]), the steady laminar diffusion flamelet model with unity Lewis numbers is used for the turbulence-chemistry interaction along with the GRI-Mech 3.0 model [30]. A presumed PDF with a beta distribution is used to model the unresolved mixture fraction fluctuations in this implementation, while a delta function is used for the scalar dissipation rate. This model's parameterization of flamelets using the mixture fraction and scalar dissipation rate at the stoichiometric mixture fraction, the latter being linearly related to the characteristic strain rate formulation we use (Eq. (2)), allows for uncertain solutions that are theoretically directly coupled to information contained in the subspaces discovered from the (a, Z) flamelet table used in Section 2.1. Additional discussion of the model formulations are available in [50], while validation of the simulation results is provided in Section 3.2.

3. Results and discussion

We begin in the following subsections by presenting results of the neural network surrogate model and active subspace generation process, along with discussion of the accompanying kinetic insights and comparisons against related work. We then present validation of the turbulent simulation used for forward uncertainty propagation, both in mesh refinement consistency and in consistency with experimental and computational results from the literature. Next, we examine and discuss how the simulation uncertainty's dependence on the various subspace directions varies substantially when evaluated at different locations in the turbulent combustion simulation domain, highlighting the versatility of the multi-target subspace generation process. Finally, we present the results of the subspace-enabled efficient forward uncertainty propagation in the turbulent simulation and compare its accuracy against the estimated ground truth.

3.1. Kinetic subspace results

Recalling that we use a neural network surrogate model trained on perturbed flamelet solutions in Cantera to accelerate the kinetic reduction, we first present in Fig. 4a comparison between the network-generated solutions and Cantera solutions for out-of-sample testing cases at various strain rates spanning three orders of magnitude. The agreement is very strong overall, with the highest observable error occurring near the fuel inlet for the low strain case, and near the peak temperature region for the highly strained case.

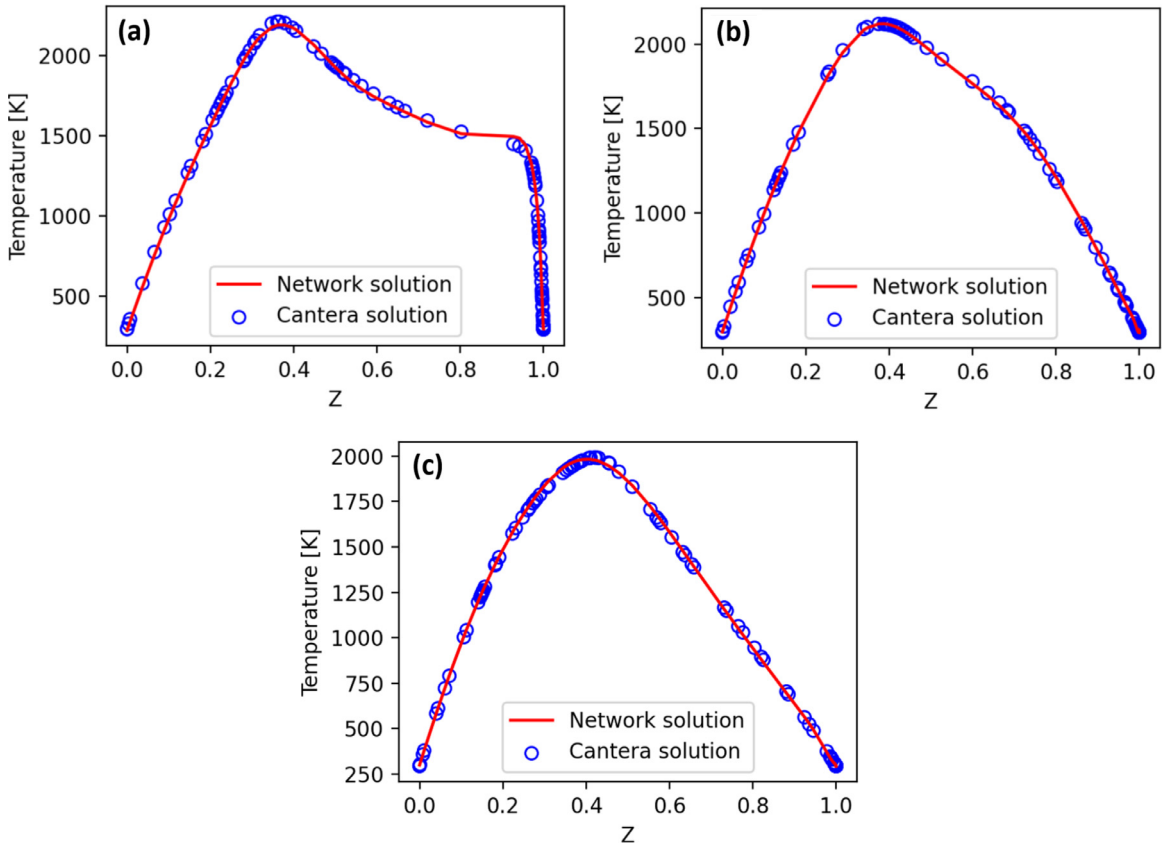

Fig. 4. Network temperature evaluation on the out-of-sample testing data at the end of the training, shown for a broad range of strain rates across three orders of magnitude: **(a)** 0.088 s^{-1}, **(b)** 3.3 s^{-1}, and **(c)** 93 s^{-1}.

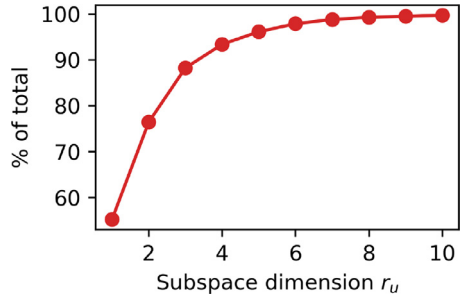

Fig. 5. Percentage of variance across all local subspaces captured by global subspaces with variable dimension r_u, computed through the percentage of all squares of singular values of **A** in the sum up to a given index. Here, we select $r_u = 3$ for 88% accuracy to the local subspaces.

Using the inexpensive gradient evaluations provided by this trained network, we implement the kinetic subspace discovery algorithm outlined in Section 2.1. We evaluate Eq. (5) once at each mixture fraction and strain rate pair using 500 kinetically perturbed samples, then use the SVD in Eq. (6) to reduce globally across the entire flamelet table. The percentage of local subspace information captured by various sizes of global subspace, computed using the square of the singular values, is reported in Fig. 5. A percentage of 100 at r_u would indicate that subspace variation across **A** could be represented entirely by the set of directions up to r_u. Here, we choose $r_u = 3$ for the remainder of this work to compromise between more directions for high accuracy and fewer directions for efficient forward propagation. At this point, we have identified the multi-target, low-dimensional subspace to be used in the forward propagation of kinetic uncertainty in the turbulent combustion simulation of Section 3.4. The remainder of the current subsection involves a detailed report of the kinetic composition of the identified three-dimensional global subspace, as well as a discussion of the mixture fraction and strain rate dependences of the eigendecomposition and SVD used to arrive at this final subspace. These analyses respectively support the proposed cost reduction attached to the active subspace method, as well as the requirement for multi-target reduction methods when handling multidimensional flow fields.

In Fig. 6, we plot the kinetic components of the final three subspace directions, as well as the activity scores computed from the SVD of Eq. (6) as per the following equation adapted from [51],

$$\alpha_\ell = \sum_{m=1}^{d} \sigma_m^2 w_{m,\ell}^2, \tag{7}$$

where the activity score α for each reaction ℓ is essentially a sum of the square of the subspace components $\mathbf{w}_{m,\ell}$, weighted by the corresponding squared singular value σ^2. Fairly rigorous mathematical and simulation-based verification in [51] supports the use of activity scores as a global sensitivity metric, which we leverage here to discuss a major advantage of the active subspace approach when compared to traditional sensitivity analysis-based reaction perturbations.

According to these activity scores, R37 is the most important for the forward propagation of uncertainty. However, it fails to capture even half of the global temperature variance as defined by the activity score. The next four reactions each account for between four and six percent of the total variance, with a further seven capturing between one and three percent each. In fact, it takes the set of the thirteen most sensitive reactions to even capture 75% of the total variance present across the flamelet table. In contrast, the ac-

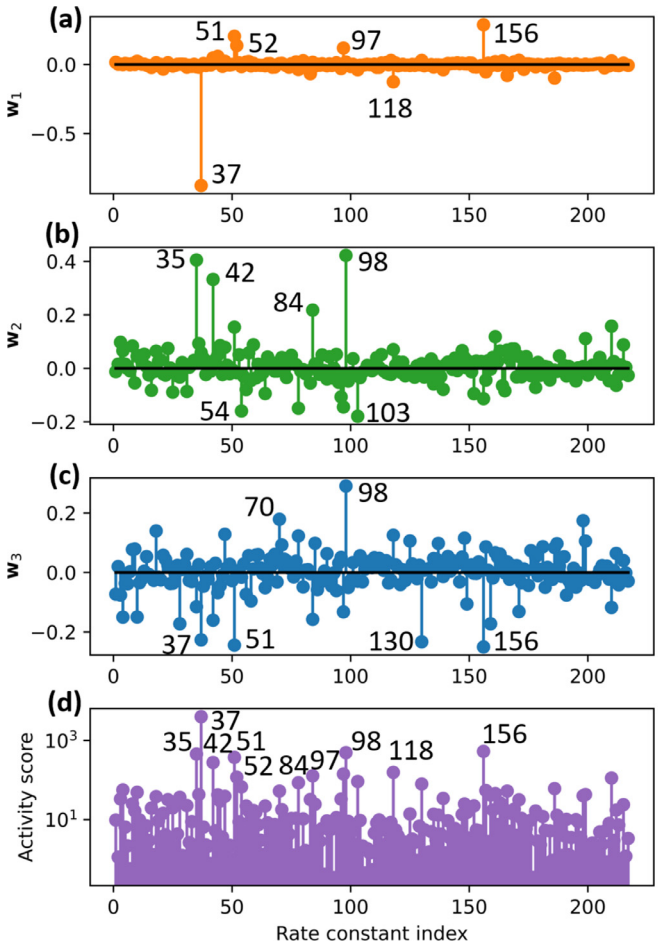

(e)

Index	Dominant Subspace(s)	Reaction
37	● ●	H + O2 [=] O + OH
156	● ●	2 CH3 (+ M) [=] C2H6 (+ M)
98	● ●	OH + CO [=] H + CO2
35	●	H + O2 + H2O [=] HO2 + H2O
51	● ●	H + CH3 (+ M) [=] CH4 (+ M)
42	●	H + OH + M [=] H2O + M
118	●	HO2 + CH3 [=] OH + CH3O
97	●	OH + CH4 [=] CH3 + H2O
84	●	2 OH (+ M) [=] H2O2 (+ M)
52	●	H + CH4 [=] CH3 + H2
103	●	OH + CH3OH [=] CH2OH + H2O
130	●	CH + CO (+ M) [=] HCCO (+ M)
54	●	H + HCO [=] H2 + CO
70	●	H + C2H2 (+ M) [=] C2H3 (+ M)

Fig. 6. Kinetic analysis based on the first three global subspace directions and activity scores. **(a)** $\mathbf{w}_1$, **(b)** $\mathbf{w}_2$, **(c)** $\mathbf{w}_3$, and **(d)** activity scores. The top six reactions in each direction are labeled in subspace direction plots, and the top ten overall sensitive reactions are labeled in the activity score plot. **(e)**: Reactions corresponding to each index labeled in **(a-d)**, in order of activity score. Dominant subspaces are reported according to the labeled reactions in **(a-c)**. Only four reactions appear in these rankings for more than one subspace and none appear in all three, indicating the relatively large set of sensitive reactions spread over these three subspace directions.

tive subspace method's exploration of sensitivity directions instead of sensitivity indices allows for greater compression of information. We observe that the first active subspace direction $\mathbf{w}_1$ is largely dominated by the key R37, but that the second and third directions $\mathbf{w}_2$ and $\mathbf{w}_3$ contain perturbations of many of the remaining key reactions compressed into fewer sensitivity directions. While perturbing these sensitive reactions themselves would require the exploration of a kinetic space of dimension greater than ten in order to achieve fair accuracy, with just three active subspace directions we are able to very efficiently explore the same uncertainty space with fewer required turbulent simulations.

We additionally report on the strain dependence of the local kinetic subspaces. It was found in [28] that the local kinetic subspaces varied strongly across the mixture fraction space of a single flamelet, which originally motivated the SVD from Eq. (6) for the construction of a global subspace. The authors of that work cited the result of [52], which showed that kinetic sensitivity directions did not change with strain rate, and proposed that their subspace constructed from a flamelet at a highly strained condition might apply across the entire flamelet table. We report various strain rate-dependent local subspace quantities in Fig. 7 to test this hypothesis. In Fig. 7a, we see that as the strain rate moves away from the extinction value, it becomes more and more difficult to capture a significant portion of the local sensitivity information in a single subspace direction. The choice of uniformly one-dimensional subspaces was justified fairly rigorously in the high-strain case of [28], though as we move to include all strained cases in this work this rigorous justification no longer holds. Instead, we show in the supplemental Fig. S3 that the bulk of the uncertainty in the flamelets occurs in the regions of the (a, Z) domain where a one-dimensional local subspace dominates the uncertainty response, according to the result of Fig. 7a, and that the regions of Fig. 7a that demonstrate a need for greater than one subspace direction contain relatively little of the temperature uncertainty. The lower temperature uncertainty magnitude seen in the generally lower-strain regions can be physically interpreted as a shift away from kinetics and toward equilibrium chemistry, making accurate kinetic uncertainty quantification in these areas less essential for overall performance. Thus, by adding additional local subspace directions to the areas of Fig. 7a that cannot be captured well with a single direction, the resulting global subspace would skew more toward the regions of the flamelet table with relatively less kinetic sensitivity importance, and may result in lower performance than if a single local subspace direction was used at all points in the flamelet table. The validity of this theory is demonstrated in the turbulent simulation later in Section 3.4. We proceed currently with the kinetic reduction process using one-dimensional local subspaces across the full (a, Z) domain.

In Fig. 7b, the kinetic similarity is seen to be preserved fairly well in the highly strained range leading up to extinction, corroborating the conclusion of [52] that for near-extinction flamelets the kinetic sensitivity does not depend on the strain rate. Below this

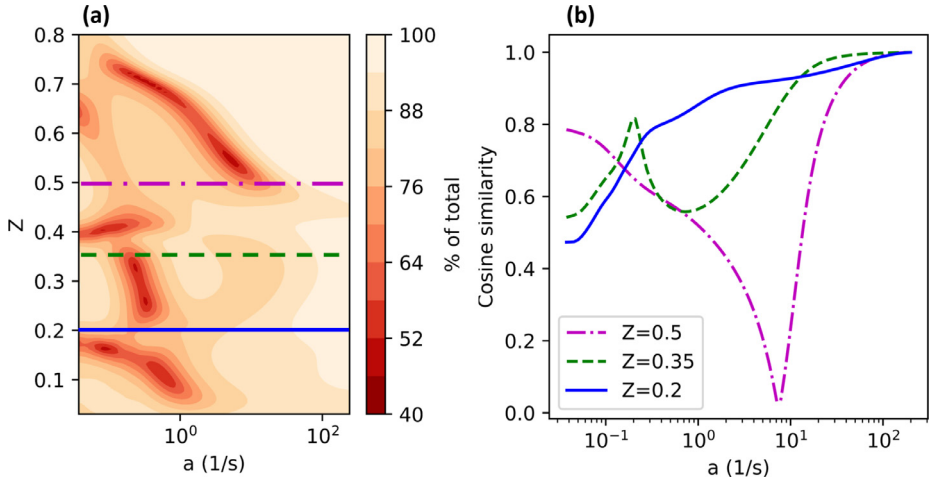

Fig. 7. **(a)** Percent of sum of all eigenvalues represented by the first eigenvalue from Eq. (5), describing the variation in gradient information that can be captured by a single subspace direction at each (a, Z) coordinate in the flamelet table. The stoichiometric mixture fraction here is $Z = 0.351$. **(b)** Strain dependence of the cosine similarity of local kinetic subspaces at three sampled mixture fractions when compared to the near-extinction strain rate. Values near unity are observed in the high-strain region, while as the strain is further reduced the kinetic similarities decrease substantially.

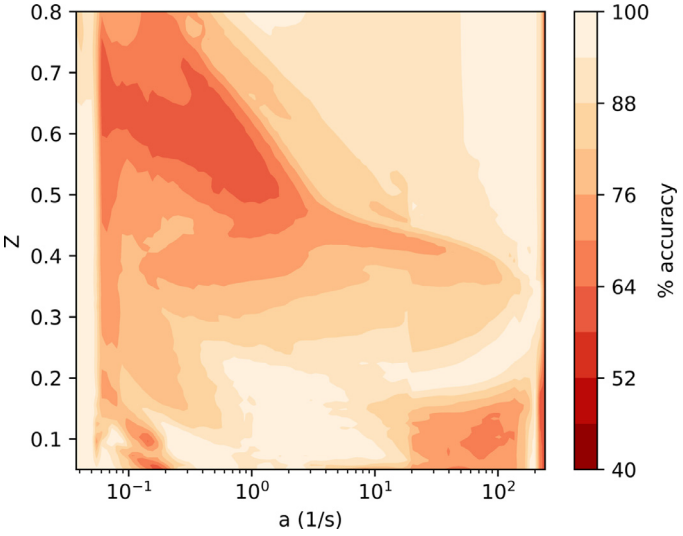

Fig. 8. Accuracy of the three-dimensional global subspace at each local (a, Z) in the flamelet space, measured by agreement in uncertainty quantiles when compared to full-dimensional uncertainty ranges.

point, however, as we move into the lower strain rates that were not considered in [52], we observe that the similarity in kinetic sensitivity breaks down significantly at all three sampled mixture fractions - stoichiometric, fuel side, and oxidizer side. Further details regarding these shifts in kinetic sensitivity and the large number of sensitive reactions present when investigating the entire flamelet table are available in Table S2 and Figure S2 of the supplementary material. It is this breakdown of similarity that calls for the two-dimensional reduction step detailed in Section 2.1.

Next, we investigate the accuracy of this three-dimensional subspace in predicting the temperature uncertainty in the flamelets. We use the same methodology as is used in [28] to compare perturbed flamelet solution profiles in the subspace against those in the full kinetic parameter spaces, using the percent error between the magnitude of the temperature uncertainty ranges derived from the subspace-perturbed solutions against the fully perturbed solutions to gauge the accuracy of the subspace. We plot these accuracies locally at each mixture fraction and strain rate in Fig. 8 and observe a similar trend to that of Fig. 7a, where at lower strains the three-dimensional subspace is not able to predict the temperature uncertainty as well as at higher strains. The difference in the exact shape of these two plots is likely due to shared information or a lack thereof across subsets of the (a, Z) domain - that is, the existence of local one-dimensional subspaces across a swath of the domain does not imply similarity across such one-dimensional subspaces, and conversely a swath of the domain with poor one-dimensional behavior does not necessarily imply the dissimilarity of these multidimensional subspaces. Such discrepancies are evident in Fig. 7b when comparing the fuel-rich slice against the stoichiometric and lean slices at mid-range strain rates. Regardless of the minutiae of such a comparison, we note the overall accuracy here defined by mean absolute error is 85%, which corresponds fairly well to the 88% accuracy to the local subspaces that we predicted in Fig. 5. We conclude that even with the strain-based discrepancies seen in Fig. 7a, three subspace directions are still sufficient to largely capture the temperature uncertainty in the flamelet table. In the following sections, we shift to discuss the three-dimensional subspace's predictive capabilities in the scaled-up turbulent combustion simulation.

3.2. Turbulent simulation validation

Here we briefly present validation of the turbulent combustion simulation used in the following sections. The mesh size is evaluated through the refinement test in Fig. 9a-b, motivating use of 24,180 cells in later applications. The converged results were then verified against the model results of [47] and the experimental data of [53], in Figs. 9c through 9h.

3.3. Spatial dependence of kinetic sensitivity

With a finalized three-dimensional kinetic subspace and a verified turbulent model, we move next to analysis of the spatial variation of kinetic sensitivity directions in the turbulent flame. To begin, we establish a baseline result by sampling the full-scale uncertain kinetics and generating solution profiles for 2000 kinetic perturbations. The statistics have not yet fully converged with 2000 samples, though to save on computational effort we refer to the result found in [1], where 2000 flamelet samples was reported as a lower bound for good performance in the same physical problem with a similar flamelet model and an identical chemical reaction model. We additionally emphasize that these samples are not

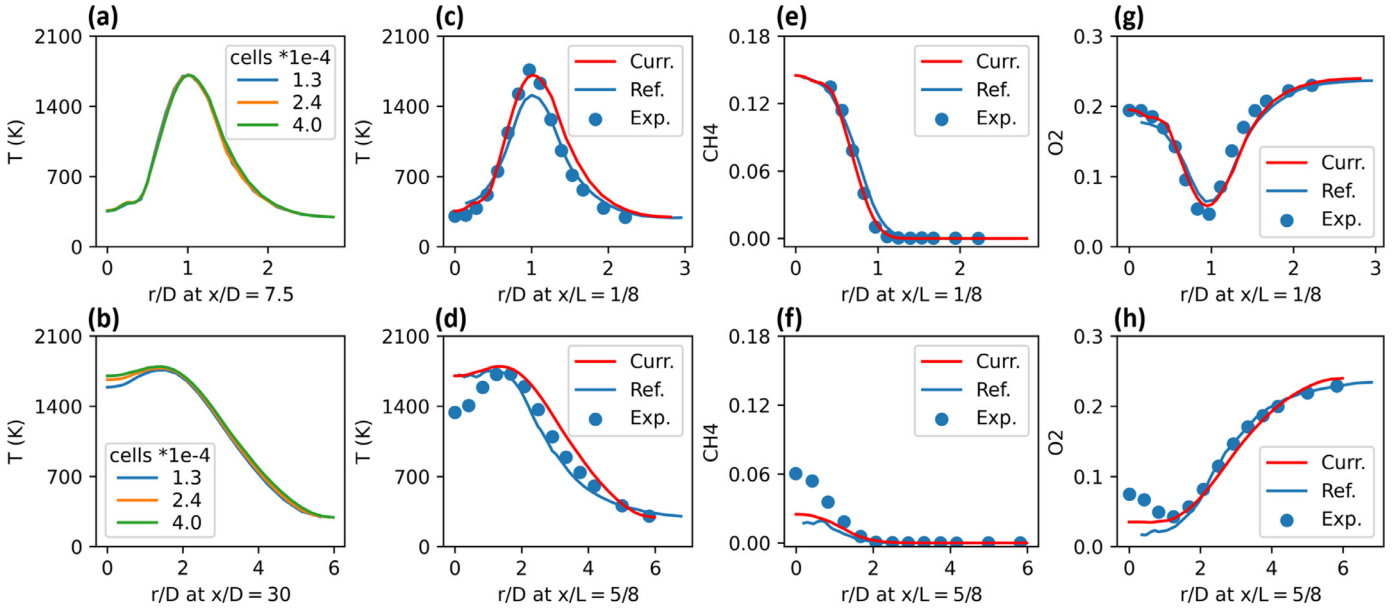

Fig. 9. Validation of the current Sandia Flame D simulation. **(a-b)** Grid convergence results of temperature slices at $x/D = 7.5$ and $x/D = 30$ on top and bottom, respectively. 24,180 cells used henceforth. **(c-h)** Validation against computational [47] and experimental [53] results in the literature for **(c-d)** temperature, **(e-f)** methane mass fractions, and **(g-h)** oxygen mass fractions. The top plots show comparisons at $x/L = 1/8$, and the bottom at $x/L = 5/8$, where $L = 1.2m$ is the full length of the computational domain.

required for the proposed subspace-powered forward uncertainty quantification in the turbulent simulation. They instead serve to help us visualize how the uncertainty in the full kinetic space reacts to each subspace, and propose accuracy values for the efficient subspace-driven forward uncertainty solutions shown later in Section 3.4. This type of detailed spatial analysis and accuracy prediction was not possible in [1] due to the more accurate and more expensive large eddy simulations used, as well as the previously discussed difference in approach to kinetic reduction.

The summary plots in Fig. 10 show how the maximum temperature at the centerline and maximum temperature at the $x/D = 30$ slice in the turbulent simulation change with motion along the three subspace directions. Such motion is characterized by the dot product between the given subspace direction and the randomly perturbed kinetic parameter vectors (which in this section are sampled from the full, 217-dimensional kinetic uncertainty space). A perfect one-to-one functional mapping of temperatures to motion along a single subspace direction would indicate that such a one-dimensional subspace is able to fully explain all of the target temperature variation, regardless of motion along the other 216 kinetic directions contained in each sample. Alternatively, an uncorrelated, cloud-like shape in such a mapping indicates that those other 216 kinetic directions substantially affect the temperature response, and thus the investigated subspace is not able to unilaterally predict the temperature response well. We see from the two-dimensional summary plots, moving from the top toward the bottom, that the centerline maximum temperature is not correlated with movement in direction $\mathbf{w}_1$, which is fairly surprising given the relative dominance of $\mathbf{w}_1$ from Fig. 5. On the other hand, the response of the maximum temperature of the near-nozzle slice responds extremely well to $\mathbf{w}_1$. Both temperatures respond fairly well to $\mathbf{w}_2$, though the centerline temperature has a tighter spread and can thus be said to more closely align with motion in the $\mathbf{w}_2$ direction. The centerline temperature responds fairly strongly to $\mathbf{w}_3$, while the near-nozzle slice has a much weaker and interestingly inverse relationship with $\mathbf{w}_3$. Finally, when we choose the strongest pair of subspaces for the bottom set of Fig. 10 plots showing temperature responses to coupled inputs, we see convincing two-dimensional behavior in both cases. We note, however, that the meaningful two-dimensional behavior is observed in $\mathbf{w}_2$ and $\mathbf{w}_3$ for the centerline maximum temperature and conversely $\mathbf{w}_1$ and $\mathbf{w}_2$ for the axial maximum temperature, following from the above discussion. We also note stronger overall correlation to the three subspace directions of the near-nozzle temperature values compared against that of the centerline temperature values, seen most clearly when comparing Fig. 10a against 10f, or 10d against 10h. This trend is unsurprising in light of the results shown in Fig. 8, where stronger performance in the flamelets was observed at higher strain rates (corresponding to upstream, near-nozzle sampling in the turbulent simulation), and lower performance in the flamelets was observed at lower strain rates (correspoinding to downstream regions). However, it does emphasize the direct coupling of the flamelet table and the turbulent simulation, suggesting that prior error estimates based on flamelet results are possible not only globally, but also locally across the axial coordinate of the turbulent domain.

The key takeaway from these summary plots is that the kinetic dissimilarity noted in the flamelet mixture fraction space in [28] as well as in the strain rate space in Fig. 7 appears to substantially propagate forward to the turbulent combustion simulation. When we sample temperatures near the nozzle, we see responses that are strongly coupled to $\mathbf{w}_1$, which as we recall from Fig. 6 is dominated by R37. Further downstream, however, this dependence appears to become nearly negligible, and the maximum temperature response is instead tied strongly to $\mathbf{w}_2$ and $\mathbf{w}_3$, which are made up of linear combinations of a much more diverse set of reactions. This spatially dependent result further highlights a drawback of the traditional, single-target combustion applications of the active subspace algorithm when the uncertainty target is a continuous profile and not simply a scalar value. We observe additionally (in Fig. 6) that there is no substantial overlap in key reactions across these three subspace directions. It is thus not simply a shifting dependence in a small set of key reactions that we observe, it is instead a shift in the list of key reactions themselves that is occurring across the turbulent flame. This makes sensitivity index-based forward propagation more expensive due to the inflated number of sensitive reactions when considering the entire solution domain, an issue that is not observed here thanks to the greater dimensional compression offered by the active subspace.

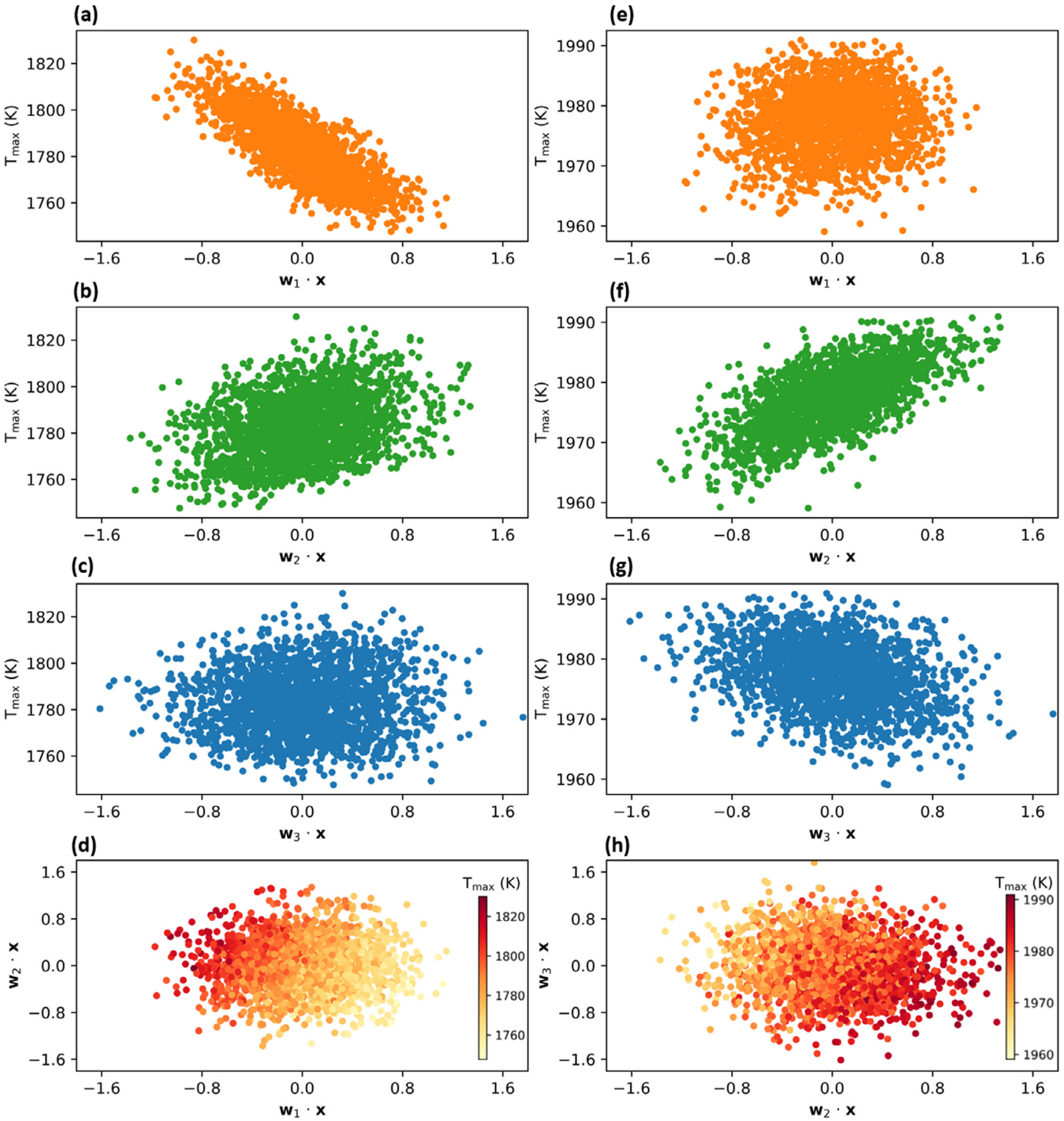

Fig. 10. Summary plots showing the response of **(a-c)** the near-nozzle ($x/D = 30$) maximum temperature and **(e-g)** the centerline maximum temperature to motion along the $\mathbf{w}_1$, $\mathbf{w}_2$, and $\mathbf{w}_3$ subspace directions, respectively. **(d)** and **(h)** show coupled responses of the respective temperature values to motion along two subspace directions. Based on the substantial shifts in the dominant subspace directions seen across each pair in the top six subplots, the axes in **(d)** and **(h)** are $\mathbf{w}_2$ vs. $\mathbf{w}_1$ and $\mathbf{w}_3$ vs. $\mathbf{w}_2$, respectively.

3.4. Efficient uncertainty quantification using kinetic subspace

In this section, we investigate the accuracy of kinetic perturbations within the three-dimensional subspace when applied to the forward problem in the Sandia Flame D simulation. In the previous section, we discussed the need for greater than 2000 samples in the full kinetic space in order to converge the statistics of the turbulent simulation. Here, we sample directly within the uncertainty space defined by the three-dimensional subspace (as opposed to the 217-dimensional full kinetic space), and find that with computational savings of multiple orders of magnitude we are able to reconstruct the full uncertainty profiles with strong accuracy. In Fig. 11a-b, we compare the three sigma temperature uncertainty ranges of the centerline profile and near-nozzle profile when using just seven subspace-informed Latin Hypercube samples [54] against those with the full 2000 samples,

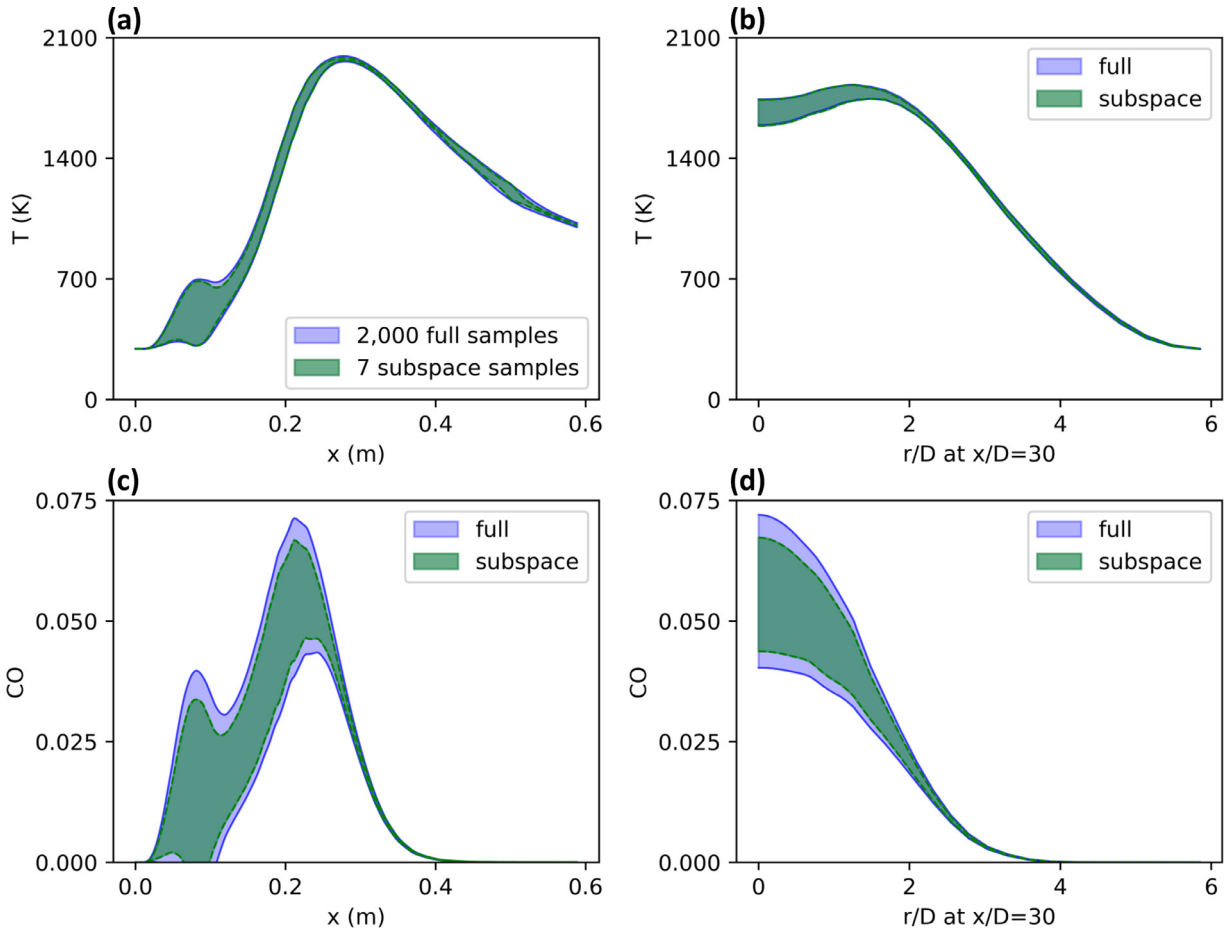

Fig. 11. Uncertainty ranges for temperature and CO mass fractions at representative locations. The estimated ground truths are from 2000 samples in the full kinetic uncertainty space. The subspace results are computed using just seven samples from the three-dimensional subspace. **(a)** Temperature uncertainty along the centerline. **(b)** Temperature uncertainty across the $x/D = 30$ near-nozzle slice. **(c)** CO mass fraction uncertainty along the centerline. **(d)** CO mass fraction uncertainty across the $x/D = 30$ near-nozzle slice.

and observe 70.4% and 82.3% accuracy, respectively, where accuracy here is defined using the percent error between the magnitude of the temperature uncertainty ranges (defined using the standard deviation) derived from the subspace-perturbed solutions against those from the fully perturbed solutions. We can trace the discrepancy in accuracy between these locations back to the results of Figs. 8 and 10 where we generally noted stronger subspace performance in the high-strain flamelets and in the axial maximum temperature, and weaker subspace performance in the lower-strain flamelets and in the centerline maximum temperature.

We additionally plot the CO mass fraction uncertainty ranges in Fig. 11c-d based on both the full 2,000-sample run as well as the subspace-reduced 7-sample run. The accuracies here were found to be 68.7% and 69.7%, respectively, for the centerline profile and near-nozzle profile. CO was not tracked in the surrogate modelling and subspace reduction process, thus all agreement here is due to the strong coupling between the temperature profile and species evolution profiles. If higher-accuracy species uncertainty profiles are desired, users can either (1) replace the temperature prediction network with a species prediction network and otherwise retain an identical methodology for a subspace that is tailored to a single species profile, or (2) increase the size of the network output layer to facilitate the learning of temperature and/or multiple species profiles, and simply add the additional species-based local kinetic subspaces into the **A** matrix as was done in this work for the strain-dependent temperature profiles. For brevity, we do not consider such generalizations in this work and instead present the extrapolation capabilities of the temperature subspace to the CO species profiles to highlight promise for such future applications.

Due to the relatively inexpensive turbulence model used in this work, we are able to repeat this subspace-informed forward uncertainty propagation multiple times to confirm the reliability of this result. We independently sampled between 7 and 50 subspace-informed perturbations for each trial. In Fig. 12, we plot the accuracy of the uncertainty ranges of each of these runs when compared against the full-space 2000 sample case. We observe greater than 70% and greater than 80% accuracy for the centerline and near-nozzle temperature uncertainty ranges, respectively, at all sample numbers. In the samples leading up to 20, there is a noisy yet overall substantial trend of increasing accuracy. Past 20, the accuracy values tend to fairly stable quantities in the $80-90\%+$ range for temperatures and the $85-95\%+$ range for CO mass fractions. There is one noticeable outlier in the axial near-nozzle temperature agreement in the 40 sample case, which we note to still achieve 82.6% and 83.9% accuracy in the near-nozzle and centerline profiles, respectively. Barring this outlier, all sample numbers saw roughly 10% better performance in reconstructing the near-nozzle temperature profile when compared against the centerline profile. This result is again not surprising given the trend of higher accuracy in higher strain regions seen in the flamelet results of Fig. 8, and later on in the turbulent simulation summary plots of Fig. 10. However, the continuation of this trend across the various metrics of Figs. 8, 10, and 12 suggest the capability of the inex-

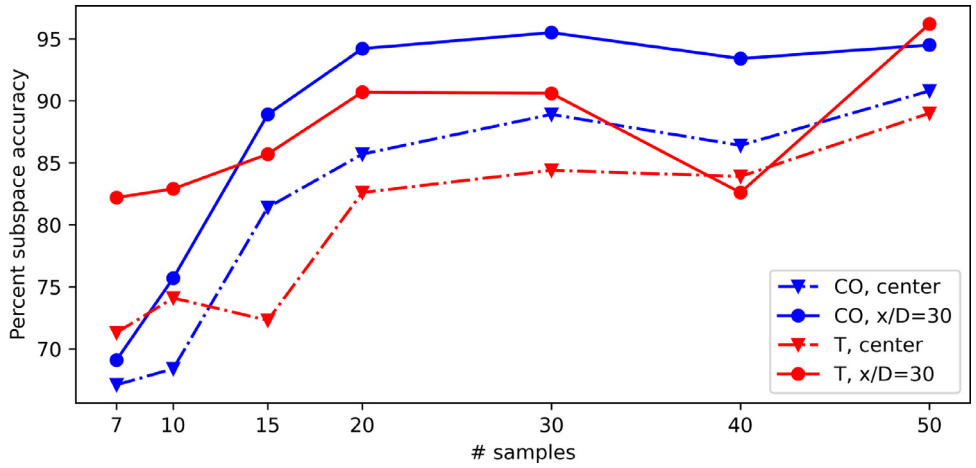

Fig. 12. Percent accuracy of small-sample subspace uncertainty ranges against the set of 2000 full model runs, calculated across various slices in the turbulent simulation domain. Temperature profile accuracies follow the pattern discussed in Fig. 10 of stronger performance closer to the nozzle. CO profiles were not included in the set of subspace targets but see strong agreement nonetheless.

pensive flamelet table statistics to effectively predict local accuracy variations in the turbulent flame via their own accuracy distributions in the (a, Z) domain.

Accuracy averages across additional experiments to verify the previously made assumption of one-dimensional local subspaces are available in the Supplemental Table S3. Results there support the hypothesis of Section 3.1 that including a second local subspace direction would dilute the high-strain, high-information areas shown in Fig. S3 that are already well-captured by uniquely one-dimensional local subspaces.

In all cases, the uncertainty reductions shown here represent a large amount of computational savings. When compared against the greater than 2000 samples needed to fully converge the uncertainty of the full kinetic space, the current subspace enables 300x fewer runs to achieve strong accuracy using just 7 samples. For cheaper simulations where the user is able to sample the subspace 30–50 times, the uncertainty ranges appear to converge with upwards of $80-90\%$ accuracy, depending on the sampling location. Large computational savings are similarly to be expected when compared against comparable or even larger chemical models than methane.

We additionally point to the sensitivity analysis results of Fig. 6, where we discussed the benefit of the active subspace method in terms of more compact dimensional representations of the key kinetic parameters. The sensitivity analysis revealed more than ten highly sensitive reactions, individual perturbations of which would not even be possible with the seven samples used as a low-end benchmark here. Thus, even in the more realistic case where the computational savings of the current method are compared against a reduced model or perturbations of highly sensitive reactions only (as opposed to the fully detailed model), our proposed framework still offers a cheaper and more substantially reduced space within which users must sample. We acknowledge that we appear to require no fewer samples than [1] in order to characterize the same Sandia Flame D temperature uncertainties, indicating no increase in savings compared to that work. However, we note that the differing reduction methodology performed here allows for accuracy estimation in the flamelet table, which we see based on Figs. 8 and 12 is a good indicator of the subspace's global accuracy in the larger turbulent simulation. The preceding discussion in this subsection also shows how the global subspace's accuracy metrics across the flamelet table can predict the spatial dependence of accuracy in the turbulent simulation, enabling local accuracy predictions in the turbulent case based on flow regime comparison against the cheap surrogate samples. This methodology finally allows for the direct relation of uncertainty responses to kinetic parameters, as was shown in Fig. 6. This tradeoff between computational cost, accuracy predictions, and kinetic interpretability is a decision that can be made based on the needs of the case at hand, though we demonstrate in this turbulent case the promise of our methodology in handling all three.

As a final note, we recall that the turbulent simulations carried out in Sections 3.2 through 3.4 to evaluate this novel kinetic reduction methodology used a flamelet-based turbulent combustion model to take advantage of the direct link to the flamelet-based subspace. However, the application of the kinetic subspaces discovered here is not strictly limited to flamelet-based models. The kinetic reduction process occurs in the kinetic parameters themselves, as opposed to directly in the flamelet solution data as was done in the highly efficient result of [1]. It is therefore possible to apply the perturbed kinetic models in a broader range of combustion regimes and models than just flamelet methods. Much like the strong kinetic uncertainty correlations found in [2] and [22] between the sensitivity of homogeneous ignition delay times and autoignited turbulent flame liftoff heights (even without a strict theoretical connection between those two scalar quantities), we theorize that our methodology will remain accurate and efficient to a certain extent even in non-flamelet-based turbulent combustion simulations thanks to the shared chemistry and flow conditions with the flamelet table. While not investigated here, we note this broader applicability for its potential in future work.

4. Conclusions

In this work, we demonstrated a complete framework for flamelet-based kinetic sensitivity reduction in a two-dimensional turbulent combustion simulation in the flamelet regime. Using a multi-target, neural network-accelerated active subspace reduction in the flamelet table, we discovered a three-dimensional kinetic subspace that was able to reconstruct the full temperature uncertainty profile of the Sandia Flame D with strong accuracy in a Reynolds-averaged, flamelet-based simulation. The accuracy of this reconstruction corresponded fairly well both globally and locally to the accuracy observed in the much cheaper flamelet simulations, allowing for meaningful a priori error estimates across the turbulent flame profile even in the realistic case where expensive convergence testing cannot be carried out in the full-scale turbulent simulation.

In addition to the strong uncertainty quantification results, the behavior of the subspaces across both the flamelet table input parameters and the turbulent simulation spatial domain revealed notable insights into the shifting kinetic sensitivity dependencies across these various input domains, which would not be possible to capture using a standard, scalar quantity of interest sensitivity method. While the kinetic sensitivities were more complex and strain rate-dependent than expected in the literature, the multi-target methodology proposed here proved to be robust and maintained high accuracy and significant dimension reduction. The temperature-based subspace is also shown to have good species profile predictive capabilities, with strong potential for further improvement when the network and subspace portions of the methodology are adjusted on a case-by-case basis to include species targets. The flexibility, multi-target applicability, predictable error ranges, low computational cost, and kinetic interpretability of this method make it a promising tool for efficient uncertainty quantification in small-scale turbulent combustion simulations similar to that which was demonstrated here, as well as in more expensive large eddy simulations.

Novelty and Significance Statement

This work developed a framework to enable efficient kinetic uncertainty quantification in turbulent combustion, especially in the flamelet regime, and demonstrates such feasibility in the benchmark Sandia Flame D simulation. It confirms the existence of and procedure to obtain low-dimensional active kinetic subspaces that dominate the response of the entire flamelet table to kinetic uncertainty, expanding on previous active subspace efforts that typically investigate the response of a single scalar output quantity only. This expanded consideration of the full two-dimensional phase space of the flamelet table is enabled by a specialized neural network surrogate model. The demonstrated methodology allows substantially more efficiency in the sampling of kinetic uncertainty for forward propagation in turbulent combustion simulations than standard sensitivity-based methods, while retaining high accuracy and strong kinetic interpretability.

Declaration of Competing Interest

The authors declare that they have no known competing financial interests or personal relationships that could have appeared to influence the work reported in this paper.

CRediT authorship contribution statement

Benjamin C. Koenig: Methodology, Investigation, Visualization, Writing – original draft. **Sili Deng:** Conceptualization, Project administration, Writing – review & editing.

Acknowledgements

SD acknowledges the support from the National Science Foundation under Grant No. CBET-2143625. BCK is partially supported by the National Science Foundation Graduate Research Fellowship under Grant No. 1745302. The authors would like to thank Dr. Weiqi Ji for thoughtful discussion during the conceptualization of this project. The authors would also like to thank Professor Michael Mueller and Professor Suo Yang for their constructive feedback regarding the flamelet modelling approach. The authors would finally like to thank Dr. Tian Tian for access to Fluent.

Supplementary material

Supplementary material associated with this article can be found, in the online version, at doi:10.1016/j.combustflame.2023.113015

References

[1] M.E. Mueller, G. Iaccarino, H. Pitsch, Chemical kinetic uncertainty quantification for large eddy simulation of turbulent nonpremixed combustion, Proc. Combust. Inst. 34 (2013) 1299–1306.
[2] W. Ji, Z. Ren, Y. Marzouk, C.K. Law, Quantifying kinetic uncertainty in turbulent combustion simulations using active subspaces, Proc. Combust. Inst. 37 (2019) 2175–2182.
[3] J.M. Armengol, O. Le Maitre, R. Vicquelin, Bayesian calibration of a methane-air global scheme and uncertainty propagation to flame-vortex interactions, Combust. Flame 234 (2021) 111642.
[4] R.E. Cornell, M.C. Barbet, J. Lee, M.P. Burke, NH3 Oxidation by NO2 in a jet–stirred reactor: the effect of significant uncertainties in H2NO kinetics, Appl. Energy Combust. Sci. 12 (2022) 100095.
[5] M.P. Burke, Harnessing the combined power of theoretical and experimental data through multiscale informatics, Int. J. Chem. Kinet. 48 (2016) 212–235.
[6] J.A. Miller, R. Sivaramakrishnan, Y. Tao, C.F. Goldsmith, M.P. Burke, A.W. Jasper, N. Hansen, N.J. Labbe, P. Glarborg, J. Zádor, Combustion chemistry in the twenty-first century: developing theory-informed chemical kinetics models, Prog. Energy Combust. Sci. 83 (2021) 100886.
[7] H. Wang, D.A. Sheen, Combustion kinetic model uncertainty quantification, propagation and minimization, Prog. Energy Combust. Sci. 47 (2015) 1–31.
[8] B. Yang, Towards predictive combustion kinetic models: progress in model analysis and informative experiments, Proc. Combust. Inst. 38 (2021) 199–222.
[9] W. Ji, J. Wang, O. Zahm, Y. Marzouk, B. Yang, Z. Ren, C. Law, Shared low-dimensional subspaces for propagating kinetic uncertainty to multiple outputs, Combust. Flame 190 (2018) 146–157.
[10] K. Konakli, B. Sudret, Polynomial meta-models with canonical low-rank approximations: numerical insights and comparison to sparse polynomial chaos expansions, J. Comput. Phys. 321 (2016) 1144–1169.
[11] Y. Zhang, W. Dong, L.A. Vandewalle, R. Xu, G.P. Smith, H. Wang, Neural network approach to response surface development for reaction model optimization and uncertainty minimization, Combust. Flame 251 (2023) 112679.
[12] M. Frenklach, H. Wang, M.J. Rabinowitz, Optimization and analysis of large chemical kinetic mechanisms using the solution mapping method-combustion of methane, Prog. Energy Combust. Sci. 18 (1992) 47–73.
[13] G. Esposito, B.G. Sarnacki, H.K. Chelliah, Uncertainty propagation of chemical kinetics parameters and binary diffusion coefficients in predicting extinction limits of hydrogen/oxygen/nitrogen non-premixed flames, Combust. Theory Model. 16 (2012) 1029–1052.
[14] M.T. Reagan, H.N. Najm, P.P. Pébay, O.M. Knio, R.G. Ghanem, Quantifying uncertainty in chemical systems modeling, Int. J. Chem. Kinet. 37 (2005) 368–382.
[15] J. Zádor, I.G. Zsély, T. Turányi, M. Ratto, S. Tarantola, A. Saltelli, Local and global uncertainty analyses of a methane flame model, J. Phys. Chem. A 109 (2005) 9795–9807.
[16] S. Li, B. Yang, F. Qi, Accelerate global sensitivity analysis using artificial neural network algorithm: case studies for combustion kinetic model, Combust. Flame 168 (2016) 53–64.
[17] Y. Tao, H. Wang, Joint probability distribution of arrhenius parameters in reaction model optimization and uncertainty minimization, Proc. Combust. Inst. 37 (2019) 817–824.
[18] D.A. Sheen, H. Wang, The method of uncertainty quantification and minimization using polynomial chaos expansions, Combust. Flame 158 (2011) 2358–2374.
[19] P.G. Constantine, E. Dow, Q. Wang, Active subspace methods in theory and practice: applications to kriging surfaces, SIAM J. Sci. Comput. 36 (2014) A1500–A1524.
[20] J.C. Sutherland, A. Parente, Combustion modeling using principal component analysis, Proc. Combust. Inst. 32 (2009) 1563–1570.
[21] S. Vajda, P. Valko, T. Turányi, Principal component analysis of kinetic models, Int. J. Chem. Kinet. 17 (1985) 55–81.
[22] N. Wang, Q. Xie, X. Su, Z. Ren, Quantification of modeling uncertainties in turbulent flames through successive dimension reduction, Combust. Flame 222 (2020) 476–489.
[23] X. Zhang, N. Wang, Q. Xie, H. Zhou, Z. Ren, Global sensitivity analysis and uncertainty quantification of soot formation in an n-dodecane spray flame, Fuel 320 (2022) 123855.
[24] P. Constantine, D. Gleich, Computing active subspaces with Monte Carlo, 2015, arXiv:1408.0545 [math].
[25] P.G. Constantine, Active Subspaces, Society for Industrial and Applied Mathematics, Pennsylvania, U.S., 2015.
[26] M. Vohra, A. Alexanderian, H. Guy, S. Mahadevan, Active subspace-based dimension reduction for chemical kinetics applications with epistemic uncertainty, Combust. Flame 204 (2019) 152–161.
[27] P.G. Constantine, M. Emory, J. Larsson, G. Iaccarino, Exploiting active subspaces to quantify uncertainty in the numerical simulation of the hyshot II scramjet, J. Comput. Phys. 302 (2015) 1–20.

[28] B.C. Koenig, W. Ji, S. Deng, Kinetic subspace investigation using neural network for uncertainty quantification in nonpremixed flamelets, Proc. Combust. Inst. 39 (2023) 5229–5238.
[29] D.G. Goodwin, R.L. Speth, H.K. Moffat, B.W. Weber, Cantera: an object-oriented software toolkit for chemical kinetics, thermodynamics, and transport processes, 2021, (https://www.cantera.org) Version 2.5.1.
[30] G.P. Smith, D.M. Golden, M. Frenklach, N.W. Moriarty, B. Eiteneer, M. Goldenberg, C.T. Bowman, R.K. Hanson, S. Song, W.C. Gardiner, Jr., V.V. Lissianski, Z. Qin, Gri-mech 3.0, (http://combustion.berkeley.edu/gri-mech/).
[31] D.A. Sheen, X. You, H. Wang, T. Løvås, Spectral uncertainty quantification, propagation and optimization of a detailed kinetic model for ethylene combustion, Proc. Combust. Inst. 32 (2009) 535–542.
[32] J. Duvall, K. Duraisamy, S. Pan, Non-linear independent dual system (NIDS) for discretization-independent surrogate modeling over complex geometries, arXiv:2109.07018 [physics] (2021).
[33] L. Lu, P. Jin, G. Pang, Z. Zhang, G.E. Karniadakis, Learning nonlinear operators via deeponet based on the universal approximation theorem of operators, Nat. Mach. Intell. 3 (2021) 218–229.
[34] J. Wang, Z. Zhou, K. Lin, C.K. Law, B. Yang, Facilitating bayesian analysis of combustion kinetic models with artificial neural network, Combust. Flame 213 (2020) 87–97.
[35] D.E. Rumelhart, G.E. Hinton, R.J. Williams, Learning representations by back--propagating errors, Nature 323 (1986) 533–536.
[36] O. Owoyele, P. Kundu, M.M. Ameen, T. Echekki, S. Som, Application of deep artificial neural networks to multi-dimensional flamelet libraries and spray flames, Int. J. Engine Res. 21 (2020) 151–168.
[37] K.M. Gitushi, R. Ranade, T. Echekki, Investigation of deep learning methods for efficient high-fidelity simulations in turbulent combustion, Combust. Flame 236 (2022) 111814.
[38] H. Chen, W. Ji, S.J. Cassady, A.M. Ferris, R.K. Hanson, S. Deng, Using shock tube species time-histories in bayesian parameter estimation: effective independent-data number and target selection, Proc. Combust. Inst. 39 (2023) 5299–5308.
[39] R. Liaw, E. Liang, R. Nishihara, P. Moritz, J.E. Gonzalez, I. Stoica, Tune: a research platform for distributed model selection and training, arXiv:1807.05118 [cs, stat] (2018).
[40] K. He, X. Zhang, S. Ren, J. Sun, Deep residual learning for image recognition, Proc. IEEE Comput. Soc. Conf. Comput. Vis. Pattern Recognit. (CVPR) (2016) 770–778.
[41] T. Fiala, T. Sattelmayer, Nonpremixed counterflow flames: scaling rules for batch simulations, J. Combust. 2014 (2014) 484372.
[42] S. Elfwing, E. Uchibe, K. Doya, Sigmoid-weighted linear units for neural network function approximation in reinforcement learning, arXiv:1702.03118 [cs] (2017).
[43] D.P. Kingma, J. Ba, Adam: a method for stochastic optimization, arXiv:1412.6980 [cs] (2017).
[44] R.S. Barlow, J.H. Frank, Effects of turbulence on species mass fractions in methane/air jet flames, Symp. (Int.) Combust. 27 (1998) 1087–1095.
[45] R.S. Barlow, J.H. Frank, Piloted CH4/Air flames C, D, E, and F release 2.1, 2007, (https://tnfworkshop.org/data-archives/).
[46] H.A.J.A. van Kuijk, R.J.M. Bastiaans, J.A. van Oijen, L.P.H. Goey, Modelling NOx–formation for application in a biomass combustion furnace, Proceedings of the European Combustion Meeting (2005).
[47] H. Wang, Y. Chen, Steady flamelet modelling of a turbulent non-premixed flame considering scalar dissipation rate fluctuations, Fluid Dyn. Res. 37 (2005) 133.
[48] C. Pfeiler, H. Raupenstrauch, Application of different turbulence models to study the effect of local anisotropy for a non-premixed piloted methane flame, Comput. Aided Chem. Eng. 28 (2010) 49–54.
[49] T.-H. Shih, W.W. Liou, A. Shabbir, Z. Yang, Jiang Zhu, A new k-epsilon eddy viscosity model for high reynolds number turbulent flows, Comput. Fluids. 24 (1995) 227–238.
[50] ANSYS Fluent Theory Guide, Release 15.0, ANSYS, Inc.(2013),
[51] P.G. Constantine, P. Diaz, Global sensitivity metrics from active subspaces, Reliab. Eng. Syst. Saf. 162 (2017) 1–13.
[52] W. Ji, T. Yang, Z. Ren, S. Deng, Dependence of kinetic sensitivity direction in premixed flames, Combust. Flame 220 (2020) 16–22.
[53] A.N. Karpetis, R.S. Barlow, Measurements of scalar dissipation in a turbulent piloted methane/air jet flame, Proc. Combust. Inst. 29 (2002) 1929–1936.
[54] M.D. McKay, R.J. Beckman, W.J. Conover, Comparison of three methods for selecting values of input variables in the analysis of output from a computer code, Technometrics 21 (1979) 239–245.